Article

Not peer-reviewed version

Synthesis and Evaluation of Antifungal and Antibacterial Abilities of Carbon Nanotubes Grafted to Poly(2-hydroxyethyl methacrylate) Nanocomposites

Karina Sandoval-García , Abraham G. Alvarado-Mendoza , Eulogio Orozco-Guareño , María A. Olea-Rodríguez , Leonardo A. Cajero-Zul , Sergio M. Nuño-Donlucas *

Posted Date: 3 August 2023

doi: 10.20944/preprints202308.0317.v1

Keywords: Carbon nanotubes; nanocomposites; poly(2-hydroxyethyl methacrylate); antifungal capacity; antibacterial ability

Article

Synthesis and Evaluation of Antifungal and Antibacterial Abilities of Carbon Nanotubes Grafted to Poly(2-hydroxyethyl methacrylate) Nanocomposites

Karina Sandoval-García [1], Abraham G. Alvarado-Mendoza [2], Eulogio Orozco-Guareño [2], María A. Olea-Rodríguez [3], Leonardo A. Cajero-Zul [4] and Sergio M. Nuño-Donlucas [4,*]

[1] Doctorado en Ciencias en Química, Centro Universitario de Ciencias Exactas e Ingenierías, Universidad de Guadalajara, Guadalajara 44430, Mexico; karina.sandoval2995@alumnos.udg.mx
[2] Departamento de Química, Centro Universitario de Ciencias Exactas e Ingenierías, Universidad de Guadalajara, Guadalajara 44430, Mexico; gabriel.alvarado@academicos.udg.mx (A.G.A.-M.); eulogio.orozco@academicos.udg.mx (E.O.-G.)
[3] Departamento de Farmacología, Centro Universitario de Ciencias Exactas e Ingenierías, Universidad de Guadalajara, Guadalajara 44430, Mexico; maria.olea@academicos.udg.mx
[4] Departamento de Ingeniería Química, Centro Universitario de Ciencias Exactas e Ingenierías, Universidad de Guadalajara, Guadalajara 44430, Mexico; leonardo.cajero@academicos.udg.mx (L.A.C.-Z.); gigio@cencar.udg.mx (S.M.N.-D.)
* Correspondence: gigio@cencar.udg.mx.

Abstract: Developing nanomaterials with the capacity to restrict the growth of bacteria and fungus is of current interest. In this study, nanocomposites of poly(2-hydroxyethyl methacrylate) (PHEMA) and carbon nanotubes (CNTs) functionalized with primary amine, hydroxyl, and carboxyl groups were prepared, and characterized. An analysis by Fourier transform infrared (FT-IR) spectroscopy and X-ray photoelectron spectroscopy showed that PHEMA chains were grafted to the functionalized CNTs. The morphology of the prepared nanocomposites studied by field emission scanning electron microscopy (FE-SEM), and transmission electron microscopy (TEM) shows significant changes with respect to the observed for pure PHEMA. The thermal behavior of the nanocomposites studied by differential scanning calorimetry (DSC) revels that the functionalized CNTs affects strongly the mobility of the PHEMA chains. Tests carried out by thermogravimetric analysis (TGA) were used to calculate the degree of grafting of the PHEMA chains. The ability of prepared nanocomposites to inhibit the growth of the fungus *Candida albicans*, and the bacteria *Staphylococcus aureus*, *Pseudomonas aeruginosa*, *Escherichia coli* was evaluated. A moderated antifungal and antibacterial capacity of the prepared nanocomposites was determined.

Keywords: carbon nanotubes; nanocomposites; poly(2-hydroxyethyl methacrylate); antifungal capacity; antibacterial ability

1. Introduction

Among the various known biomaterials, the poly(2-hydroxyethyl methacrylate) (PHEMA) stands out for its cytocompatibility, biocompatibility, and reduced immunological response from a host tissue [1]. PHEMA is a non-biodegradable, hydrophilic, stimuli-responsive, and optically transparent polymer, and it has been used extensively in the biomedical field. Their applications include hydrogel contact lens [2], cancer therapy [3], bone tissue regeneration [4], wound healing [5], neural tissue engineering [6], and controlled drug delivery systems [7], among others.

However, microbial contamination (which includes bacteria, fungi, and parasites) can limit the biomedical applications of PHEMA, because pure PHEMA does not possess antimicrobial properties [1]. Pure PHEMA cannot inhibit the growth of gram-positive and gram-negative bacteria. This drawback must be surpassed to increase the range of the biomedical potential uses of the PHEMA. Adopting effective antimicrobial strategies is necessary to achieve the safe use of polymer-based materials to make biomedical devices that improve healthcare. In this sense, the incorporation of antimicrobial drugs into PHEMA is a widely used approach [8,9]. However, implementing novel

antimicrobial strategies is of current interest, because the prevalence of antibiotic-resistant bacterial infections wakes up concerns [10].

Isolated PHEMA is rarely used. Typically, the precursor monomer (2-hydroxyethyl methacrylate) (HEMA) is copolymerized or the PHEMA is mixed with other materials to prepare a biomaterial of desirable properties. The election of a material that is added to PHEMA plays a crucial role in the properties of a PHEMA-based prepared material. Nanostructured materials can be used as nanoscale-level reinforcements of polymers. Carbon nanotubes (CNTs) are materials with outstanding physical and chemical properties and had been used as reinforcement agents of polymers to prepare nanocomposites. PHEMA-based nanocomposites reinforced with CNTs have been prepared and studied in previous works. For instance, HEMA was polymerized on the surfaces of the multi-walled carbon nanotubes (MWCNTs) by free-radical polymerization using 2,2'azo bis(isobutyronitrile) (AIBN) as initiator. The reaction product of this polymerization was studied by Fourier-transformed infrared (FT-IR) spectroscopy and was detected that chains of PHEMA were attached to the surface of MWCNTs [11]. In other work, PHEMA/MWCNTs nanocomposites were prepared by solvent casting method, specifically by the addition of PHEMA to a dispersion of MWCNTs in DMF. After the elimination of the solvent, a homogeneous dispersion of the MWCNTs was obtained. The prepared nanocomposites showed some mechanical properties higher than pure PHEMA, and better thermal stability [12].

CNTs can act as antibacterial agents [13]. CNTs have unique hexagonal structures and a high length-to-diameter ratio (for instance, up to 136,000,000:1) [14]. Besides, some of its properties (electrical, thermal, and mechanical) are better than those of other materials. However, the hydrophobic characteristics of the CNTs, and their ability to form strong van der Waals interactions among them, inhibit their dispersion in solvents and aqueous media. Because the development of novel antimicrobial materials with inhibitory bacterial capacity is an imperative necessity [15], research focused on the use of CNTs in the preparation of novel antibacterial materials is of current interest. Polymeric nanocomposites reinforced with CNTs can be used as antimicrobial agents. The main challenge to overcome for the use of CNTs-based nanocomposites as antimicrobial materials is to inhibit the natural self-aggregation of the CNTs, improve their dispersion, especially in water [16], and reduce their toxicity. In this sense, to prepare an effective antimicrobial polymeric nanomaterial containing CNTs, achieving the chemical functionalization of the CNTs is a desirable goal. Functionalized CNTs (f-CNTs) can be attached to polymeric chains reducing their natural tendency to self-aggregation and toxicity. Several types of chemical groups can decorate the surface of the CNTs, for instance, cationic group (as $–NH_2$), which inhibits bacterial growth when they have present at high concentrations, while CNTs functionalized with anionic (–COOH) and neutral (–OH) groups have strong biocide properties (7-log reduction) against some pathogens [16,17]. Moreover, when high dispersion driven by the formation of chemical bonds between f-CNTs and polymer chains is achieved, homogeneous nanomaterials are obtained as was reported elsewhere [18]. Homogeneous f-CNTs-based nanomaterials with microbial inhibitory capacity are desirable materials in the nanomedicine field.

The aim of this study was to synthesize and characterize nanocomposites of functionalized CNTs with primary amine, carboxyl, and hydroxyl groups and PHEMA, and to evaluate their antibacterial capacity. To the best of our knowledge, the chemical pathway used in this study to attach the prepared functionalized CNTs to the PHEMA chains has not been reported previously. The obtained nanocomposites were characterized by Fourier-transformed infrared (FT-IR) spectroscopy, X-ray photoelectron spectroscopy (XPS), field emission scanning electron microscopy (FE-SEM), transmission electron microscopy (TEM), differential scanning calorimetry (DSC), and thermogravimetric analysis (TGA). In addition, the ability of pure PHEMA and their nanocomposites against the growth of bacterial strains such as *Staphylococcus aureus* ATCC 6538, *Pseudomonas aeruginosa* ATCC 9027, *Escherichia coli* ATCC 25922, and the fungus *Candida albicans* ATCC 10231 was assessed.

 doi:10.20944/preprints202308.0317.v1

2. Materials and Methods

2.1. Materials

Poly(2-hydroxyethyl methacrylate) of molecular weight (Mw = 20000), trimethylamine (Et_3N, 99%), oxalyl chloride (OxCl, 98%), dichloromethane (ACS reagent), ethylenediamine (EDA, >99%) and potassium bromide (KBr, FT-IR grade (>99%)) were provided from Sigma-Aldrich (Saint Louis, MO, USA). Alumina boats were acquired from Alfa Aesar (Tewksbury, MA, USA). Nitrogen gas (99.99%) was obtained from INFRA (Guadalajara, Mexico). Argon gas (99.998% was obtained from PRAXAIR (Guadalajara, Mexico). Ferric nitrate nonahydrate ($Fe(NO_3)_3 \cdot 9H_2O$, hydrochloric acid (ACS reagent), and ethanol (99.9%) were purchased from Golden Bell (Guadalajara, Mexico). Deionized and distilled water was purchased from Productos Selectropura (Guadalajara, Mexico). Müeller-Hinton agar was acquired from MCD LAB (Tlanepantla, Mexico). Trypticase in soy agar and in soy broth were obtained from BD Bioxon (Ciudad de Mexico), Mexico. All of the chemical reagents were used without purification.

2.2. Synthesis, purification, and chemical functionalization of the CNTs

CNTs were prepared through the CVD method using ethanol as a carbon source. For this, an experimental procedure used previously by our group was followed. This procedure was reported elsewhere [19]. To achieve the purification of the prepared CNTs a mixture of concentrated HNO_3 (37.5 wt.%) diluted in water (1:3 v/v) was used. Additionally, the chemical functionalization of purified CNTs with $–NH_2$, –COOH, and –OH groups was carried out following an experimental procedure of three steps. Both procedures were developed and used by our research group previously and were reported elsewhere [20]. The experimental procedure used to functionalize the purified CNTs (named $CNTs_{pu}$) is resumed next: (i) dry $CNTs_{pu}$ were partially oxidized. As a product of the oxidation process hydroxyl, and carboxyl groups were attached to the $CNTs_{pu}$ surface. The contents of hydroxyl and carboxyl groups were calculated through two experimental procedures reported separately elsewhere. [21,22] (ii) Partially oxidized CNTs (named $CNTs_{ox}$) reacted with OxCl with the goal to attach acyl chloride functionality onto the $CNTs_{ox}$ surface. Immediately, that the product (named $CNTs_{OCl}$) was obtained, a third step was performed. (iii) $CNTs_{OCl}$ were reacted with EDA to attach amine groups at the ends of emerging side chains. The CNTs containing hydroxyl, carboxyl, and terminal amine groups (named $CNTs_{amine}$) were used to prepare the PHEMA/$CNTs_{amine}$ nanocomposites.

2.3. Synthesis of $CNTs_{amine}$/PHEMA nanocomposites

The PHEMA/$CNTs_{amine}$ nanocomposites were synthesized following a procedure of four steps. Table 1 lists the name assigned to identify each nanocomposite, and the formulations used for the preparations. Two different contents of $CNTs_{amine}$ (0.5 wt. % or 1.0 wt. %) were used in the syntheses. The description to prepare a PHEMA/$CNTs_{amine}$ nanocomposite with 0.5 wt.% of $CNTs_{amine}$ is presented next. Step 1. 1 g of PHEMA was placed into a 100-mL glass reactor. Then, 10 mL of dichloromethane was added. The dissolution was achieved by maintaining the mixture with constant stirring under a nitrogen atmosphere at room temperature (ca. 25 °C). Step 2. The reactor was immersed in an ice bath at 0 °C. Then 0.65 µL of Et_3N was added. The mixture was stirred during 20 min. Then 0.70 µL of OxCl dissolved in 5 mL of dichloromethane was added dropwise with a syringe. The mixture was allowed to react for 3 h. For this procedure, the hydroxyl groups of the PHEMA react with one acyl chloride group of OxCl, while their other acyl group can be available to react in an additional step. Step 3. 0.05 g of $CNTs_{amine}$ was added to the prepared mixture. Then, the reactor was immersed into oil bath at 30 °C. The dispersion was allowed to react for 24 h. After this, the product was introduced at oven at 30 °C until obtain a dry solid. Step 4. The product of the reaction was purified by adding 40 mL of dichlorometane and the mixture was mixed for 15 min. Next, the mixture was centrifuged at 7500 rpm. An insoluble solid (the PHEMA/$CNTs_{amine}$ nanocomposite) was recovered. Step 4 was repeated twice. When a PHEMA/$CNTs_{amine}$ nanocomposite was prepared with

Preprints (www.preprints.org) | NOT PEER-REVIEWED | Posted: 3 August 2023 doi:10.20944/preprints202308.0317.v1

1.0% of $CNTs_{amine}$ the amounts of the mentioned reagents were adjusted the maintain similar concentrations to those mentioned above. The Scheme I shows the chemical pathway used to synthesize the studied nanocomposites.

Table 1. Legends employed to identify the PHEMA/$CNTs_{amine}$ nanocomposites and the molar relationship of OxCl/hydroxyl groups used for its preparation and the content of $CNTs_{amine}$.

Identification name	**Molar relationship of OxCl/hydroxyl groups attached to $CNTs_{amine}$**	**$CNTs_{amine}$ (wt. %)**
Na 1	1/4	0.5
Na 2	1/2	0.5
Na 3	1/4	1.0
Na 4	1/2	1.0

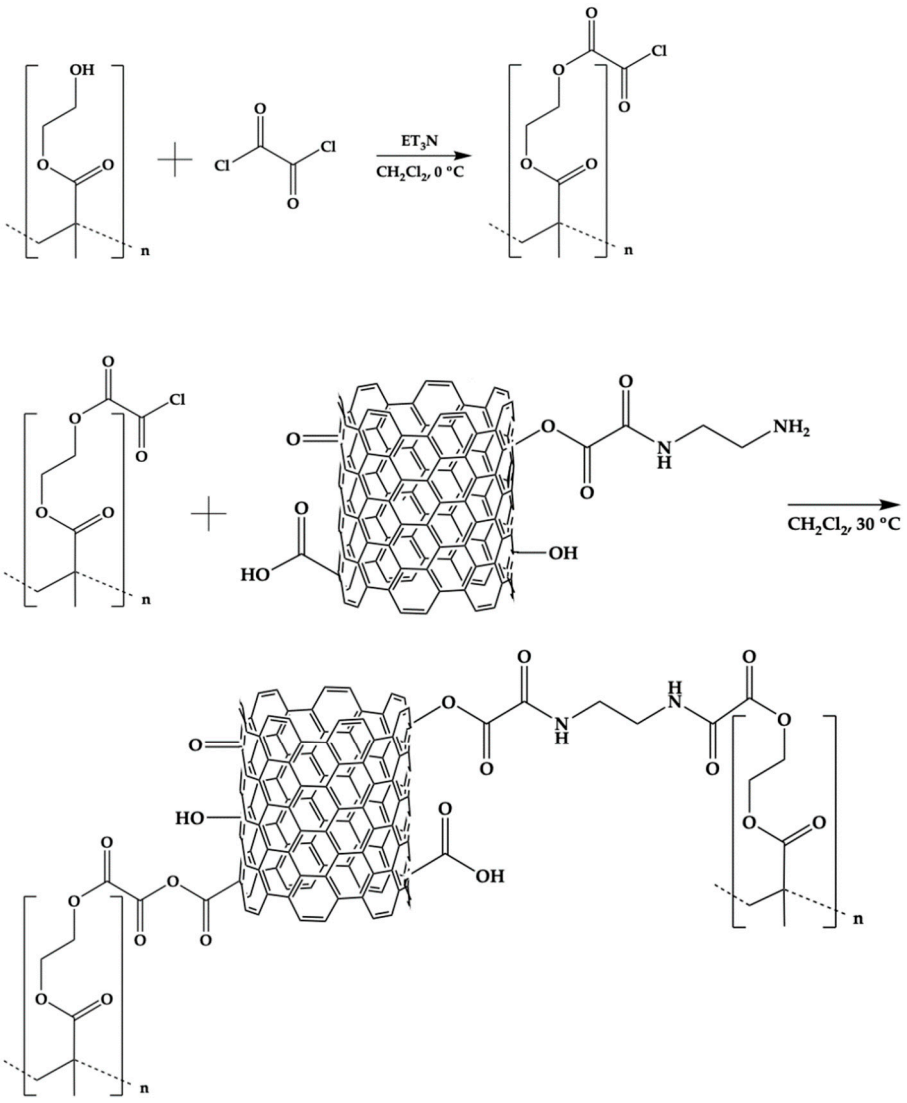

Scheme I. Chemical route followed to prepare the $CNTs_{amine}$/PHEMA nanocomposites.

2.4. Characterization of $CNTs_{amine}$/PHEMA nanocomposites

A series of experimental techniques were employed to characterize the $CNTs_{amine}$/PHEMA nanocomposites.

 doi:10.20944/preprints202308.0317.v1

2.4.1. Fourier transform infrared spectroscopy (FT-IR)

An analysis of the structure of pure PHEMA and the PHEMA/CNTs$_{amine}$ nanocomposites was carried out by Fourier-transform infrared (FT-IR) spectroscopy with an FT-IR spectrophotometer, model Spectrum One of Perkin Elmer (Waltham, MA, USA). To made the study, pellets of KBr and dry samples were prepared (at a ratio of 0.1 mg of the sample to 70 mg of KBr) by compression at room temperature (ca. 25 °C (298.15 K)). With the aim of reduce the signal/noise ratio, all reported spectra were recorded and analyzed from an average of 40 scans, and a resolution of 4 cm^{-1}. The spectra of the analyzed samples were obtained at room temperature (ca. 25 °C (298.15 K)).

2.4.2. X-Ray photoelectron spectroscopy (XPS)

Pure PHEMA and the PHEMA/CNTs$_{amine}$ nanocomposites were analyzed by X-ray photoelectron spectroscopy (XPS). To make the analysis was used equipment comprising an XR 50 M monochromatic Al Kα_1 ($h\nu$ = 1486.7 eV) X-ray source and a Phoibos 150 spectrometer with one-dimensional hemispheric detector 1D-DLD provided by SPECS (Berlin, Germany). The measurements were made at 150 W with an electron takeoff angle of 90°, a step size of 0.1 eV, and a pass energy of 10 eV. The base pressure was maintained at 4.2×10^{-10} mbar. The samples were mounted on a steel sample holder before of performed the measurements using carbon tape. A flood-gun device was employed to compensate the charges on the sample. The obtained spectra were shifted according to C-C binding energy. The data obtained were fitted using the active background approach tool of the software Analyzer v. 1.42 [23].

2.4.3. Field emission scanning electron microscopy (FE-SEM)

The morphology of pure PHEMA and the PHEMA/CNTs$_{amine}$ nanocomposites was analyzed by field emission scanning electron microscopy (FE-SEM) using a microscope model MIRA 3LU of Tescan (Brno, Czech Republic). Samples were dried in an oven at 60 °C (333.15 K) for 72 h previously to make the study. Then, ca. 0.01 g of sample was mixed with 1 cm^3 of acetone, at room temperature (ca. 25 °C (298.15 K)). The obtained mixture was sonicated for 5 min, and an aliquot of the prepared dispersion was taken with a Pasteur pipette and poured onto a Cu grid. The solvent was evaporated completely. Then, the sampled were introduced in a Baltec CE SCD004 golden evaporator, and a gold layer was created onto the sample surface. To make this, a 20 s electrodeposition process was carried out. Afterward, the sample were examined in the FE-SEM microscope.

2.4.4. Transmission electron microscopy (TEM)

Samples of pure PHEMA and the PHEMA/CNTs$_{amine}$ nanocomposites were examined with a transmission electron microscope model 1010 TEM of JEOL (Peabody, MA, USA) operated at 200 kV. Before the analysis, the samples were dried in an oven at 60 °C (333.15 K) for 72 h. Then, approximately 0.010 g of each sample was mixed with 2 mL of acetone at room temperature. Afterward, the mixture was sonicated for 5 min, and using a Pasteur pipette an aliquot of the prepared dispersion was poured onto Cu grid. The solvent was evaporated through action of a 60 W solar lamp during 20 min. Then, the sample thus obtained was analyzed.

2.4.5. Differential scanning calorimetry (DSC)

Thermal characterization of pure PHEMA and the PHEMA/CNTs$_{amine}$ nanocomposites was performed by differential scanning calorimetry (DSC) using a calorimeter model Q100 of TA Instrument (New Castle, DE, USA). Samples masses were in the range from 3 to 5 mg. DSC thermograms were obtained following a heating program from -80 °C (193.15 K) to 200 °C (473.15 K) at a heating rate of 10 K/min using a nitrogen flow rate of 50 cm^3/min. All tests were performed while maintaining an inert atmosphere. Two heating scans were recorded and the second scan is reported.

2.4.6. Thermogravimetric analysis (TGA)

Thermal analysis of pure PHEMA and the PHEMA/$CNTs_{amine}$ nanocomposites was completed through a study of thermal gravimetry analysis (TGA). The measurements were recorded in a thermobalance model TGA5000 Discovery of TA Instrument (New Castle, DE, USA) operated in the range from 25 °C (298.15 K) to 600 °C (873.15 K) at 10 K/min under a constant nitrogen flow rate of 25 mL/min to create an inert atmosphere. The masses of the samples ranged from 3 to 10 mg.

2.4.7. Evaluation of the antibacterial and antifungal abilities of pure PHEMA and the $CNTs_{amine}$/PHEMA nanocomposites

The inhibitory ability of the pure PHEMA and the PHEMA/$CNTs_{amine}$ nanocomposites against bacterial strains of *Staphylococcus aureus* ATCC 6538, *Pseudomonas aeruginosa* ATCC 9027, and *Escherichia coli* ATCC 25922 was studied. Moreover, their ability to inhibit the growth of the fungus *Candida albicans* ATCC 10231 was evaluated. The experimental procedure is described next. First, the fungus and each type of bacteria were reactivated in trypticase in soy broth with yeast extract (CSTEL) an incubated at 35 ± 2 °C (308.15 ± 2 K) for 24 h, separately. Young bacteria and fungi were obtained by two reseedings made consecutively. Second, each type of bacteria or the fungus was inoculated on Petri dishes with Müller-Hinton agar. Then the samples selected were added. The halo of inhibition was assessed after incubation at 35 °C (308.15 K) for 24 h [24].

3. Results and Discussion

As was reported previously in a study carried out by our research group [20] the surface of the $CNTs_{amine}$ was decorated with primary amine, hydroxyl and carboxyl groups. The contents of hydroxyl and carboxyl groups were 13.3 wt.%, and 37.5 wt.% respectively, per gram of the $CNTs_{ox}$ (precursor of the $CNTs_{amine}$), while the presence of the primary amine groups was documented through an analysis by FT-IR and XPS spectroscopies.

3.1. Analysis of the chemical structure of $CNTs_{amine}$/PHEMA nanocomposites

Fourier transform infrared (FT-IR) spectroscopy is an adequate technique to analyze chemical groups inserted on the walls of CNTS. FT-IR spectra of the PHEMA, Na 2, and Na 3 are shown in Figure 1. In the FT-IR spectrum of pure PHEMA (Fig 1A) were detected typical spectral contributions of this polymer reported elsewhere [25]. Thereby, the most intense band was detected at 1726 cm^{-1} and is attributed to the stretching vibration of the carbonyl bond of an ester group. The stretching vibration of the hydroxyl group produces the wide and intense band detected at 3400 cm^{-1}. Additionally, the band observed at 1160 cm^{-1} is caused by vibration of torsion of the C-H bond and symmetric stretching vibration of C-O-C functionality of the ester group. The FT-IR spectra of Na 2 (Fig. 1B) and Na 3 (Fig. 1C) show similar spectral behavior. In both spectra, significant changes with respect to the observed in the spectrum of pure PHEMA were detected. Now, additional bands are observed. Thus, at 1630 cm^{-1} a weak band attributed to the named band amide II due to vibration of flexion of the $–NH_2$ functionality of the amide group was detected. Moreover, at 1733 cm^{-1} the band of carbonyl bond of ester group was detected. As a shoulder of this band, at 1773 cm^{-1} a new band was detected, which is attributed to asymmetric stretching vibration of the two carbonyl functionalities of anhydride group. Arrows are used to identify the described spectral contributions. The formation of amide groups and anhydride groups indicate that chemical reactions carried out between acyl chloride groups added to the PHEMA, and primary amine or carboxyl groups inserted on the walls of the $CNTs_{amine}$. Through the amide and anhydride groups, chains of PHEMA are grafted to the walls of $CNTs_{amine}$ as was shown in Scheme I. It is important to mention that there is evidence of the presence of residual chemical groups of the hydroxyl, carboxyl, and C-Cl functionalities. Thus, at 3440 cm^{-1} appears a wide band due to stretching vibrations of hydroxyl groups. At 2603 cm^{-1} a wide band due to stretching vibration of O-H bond of carboxyl functionality was detected. Moreover, at 806 cm^{-1} a band caused by stretching vibration of C-Cl bond is observed.

Preprints (www.preprints.org) | NOT PEER-REVIEWED | Posted: 3 August 2023 doi:10.20944/preprints202308.0317.v1

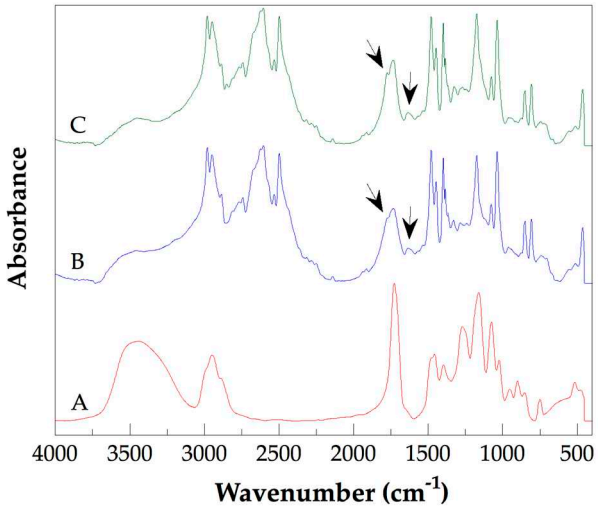

Figure 1. FT-IR spectra of PHEMA (A), Na 2 (B) and Na 3 (C).

The chemical composition and the electronic structure of PHEMA and the PHEMA/CNTs$_{amine}$ nanocomposites were studied by X-ray photoelectron spectroscopy (XPS). The analysis by XPS contributes to obtaining a better knowledge of the structure of prepared nanocomposites and provides clear information on whether a grafting reaction between the CNTs$_{amine}$ and the polymer chains of PHEMA was carried out. Figure 2 shows the *C1s* core-level normalized spectra of PHEMA and Na 1. The presented XPS spectra were adjusted to the respective shift taking as reference the signal of C-C/C-H bonds at 285.0 eV. The *C1s* core-level normalized spectrum of pure PHEMA (Fig. 2A) shows components at five positions. The components and their atomic concentrations were C–C/C–H bonds at 285.0 eV [26] (21.1%), C–C=O bonds at 285.7 eV [26] (15.2%), C–OH bonds at 286.7 eV [26] (14.6%), C–O–C bonds at 287.2 eV [26] (6.1%), and O–C=O bonds at 289.2 eV [26] (10.5%). Moreover, the *C1s* core-level normalized spectrum of Na 1 shows components also at five positions. These components and their atomic concentrations were C–C/C–H bonds at 285.0 eV [26] (29.8%), C–C=O bonds at 285.7 eV [26] (14.6%), C–OH bonds at 286.7 eV [26] (8.0%), C–O–C [26]/HN–C=O bonds [27,28] at 287.2 eV (7.2%), and O–C=O bonds at 289.3 eV [26] (6.9%). It is evident that the atomic concentration of the C-OH bonds detected in the spectrum of the Na 1 decreases with respect to that observed in the spectrum of pure PHEMA. This fact suggests that this functionality reacted. Specifically, the reaction was performed between the hydroxyl groups of the PHEMA and the acyl chloride groups of the OxCl. In a similar fashion, the slight increment of the atomic concentration attributed to C–O–C/HN–C=O bonds detected in the spectrum of Na 1 with respect to those observed in the spectrum of pure PHEMA suggests strongly that another chemical reaction takes place. Now, the well-known chemical reaction between the acyl chloride groups, and the primary amine groups to produce the amide groups was carried out. This analysis is in accordance with the described FT-IR spectra shown in Figure 1 and supports the chemical path presented in Scheme I.

Preprints (www.preprints.org) | NOT PEER-REVIEWED | Posted: 3 August 2023 doi:10.20944/preprints202308.0317.v1

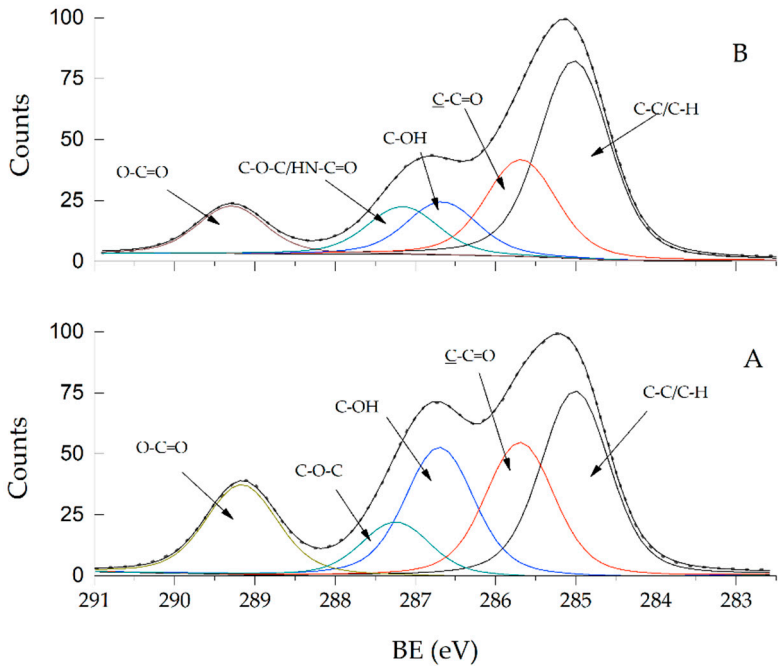

Figure 2. The C 1s core level spectra of PHEMA (A) and Na 1 (B).

Figure 3 shows the *O1s* core-level normalized spectra of PHEMA and Na 1. For the PHEMA (Fig. 3A), the *O1s* XPS spectrum shows components at three positions. The components and their atomic concentrations were O=C/O-C=O bonds at 532.7 eV [26] (13.8%), HO–C bonds at 533.7 eV [26] (12.6%), and C–O–C bonds at 534.4 eV [26] (5.2%). Similarly, the *O1s* XPS spectrum of the Na 1 also shows components at three positions. Now, the components and their atomic concentrations were O=C/O-C=O bonds at 532.7 eV [26] (14.4%), HO–C bonds at 533.8 eV [26] (6.9%), and C–O–C bonds at 534.5 eV [26] (3.1%). The most significant change between these spectra was slight the increment in the atomic composition of the O=C/O-C=O bonds detected in the *O1s* XPS spectrum of the Na 1 in comparison to detected of the PHEMA. This increment was attributed as due to a chemical reaction developed between acyl chloride groups and carboxyl groups to produce ester groups as was presented in Scheme I.

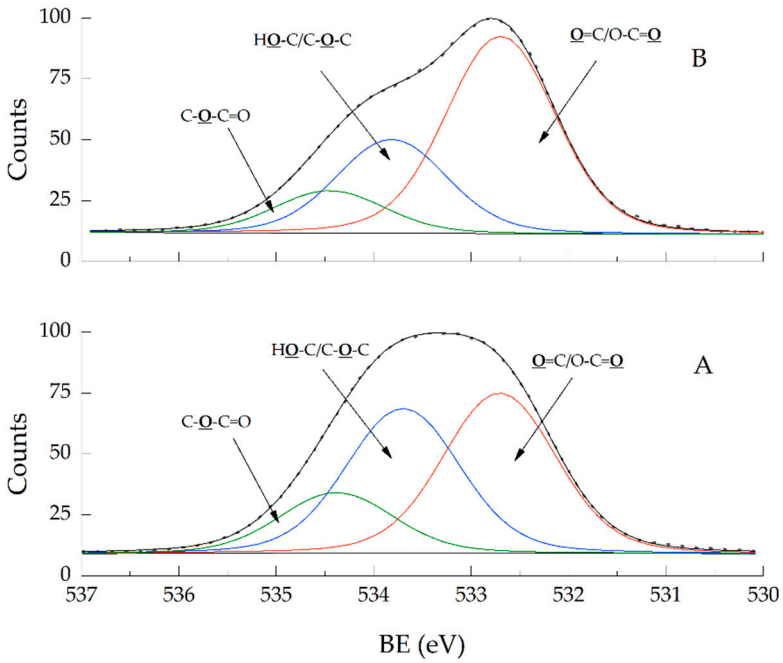

 doi:10.20944/preprints202308.0317.v1

Figure 3. The O 1s core level spectra of PHEMA (A) and Na 1 (B).

The XPS results indicate that the functionalized carbon nanotubes with hydroxyl, carboxyl, and primary amine groups are chemical attached to the polymer chains of PHEMA through amide and ester groups.

3.2. Morphological analysis of CNTs$_{amine}$/PHEMA nanocomposites

Figure 4 shows FE-SEM micrographs of pure PHEMA (Fig. 4A) and the Na 4 (Figs. 4B and 4C). The micrograph of the pure PHEMA shows a smooth surface with sharp cuts at one end. These cuts would be a consequence of the brittle nature of the PHEMA whose glass transition temperature (T_g) is higher than the room temperature (ca. 298.15 K) at which the FE-SEM analysis was performed. On the contrary, the morphology of the Na 4 shows significant changes. Now, an irregular shape morphology is observed (Fig 4B). There is an influence of the CNTs$_{amine}$ used for the preparation of the studied nanocomposite in the change of the morphology detected, as can be observed in Fig. 4C where a CNT emerging from a globular structure detected on the surface was observed. These results suggest strongly that CNTs$_{amine}$ is grafted to the PHEMA chains. In this sense, in a previous report, a significant change on the morphology of PHEMA-based nanocomposites with respect to the observed nanofiller has been explained as due to the grafting of hallosite nanotubes to the polymeric chains of PHEMA [29]. Similarly, in another study, an analysis of FE-SEM micrographs of nanocomposites of Fe_3O_4 nanoparticles/PHEMA showed a drastic change respect to the observed in micrographs of pure PHEMA. This fact was explained as due to adhesion of Fe_3O_4 nanoparticles on PHEMA chains [30].

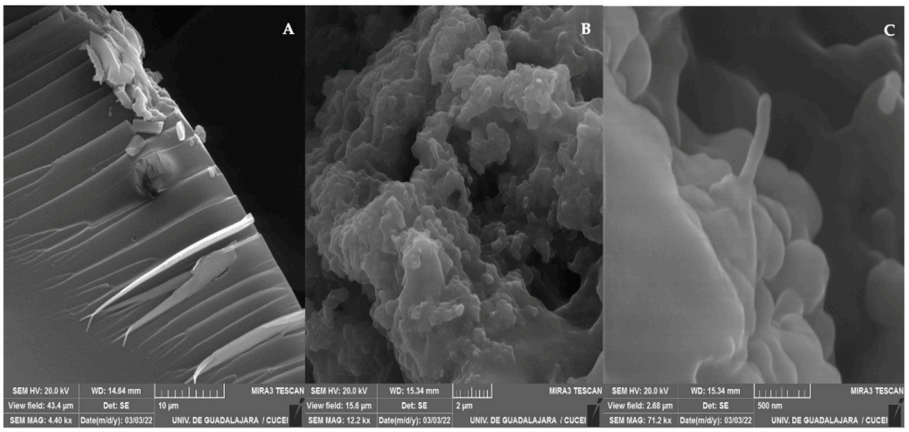

Figure 4. FE-SEM micrographs of samples of pure PHEMA (A), and the Na 4 obtained with two bars scale: 2 µm (B), or 500 nm (C).

Figure 5 depicts TEM micrographs of pure PHEMA (Fig. 5A) and Na 4 (Fig. 5B). The TEM micrograph of pure PHEMA shows darker domains, which indicate the overlapping of layers of PHEMA [31]. Moreover, can observe circular regions probably formed during the evaporation of the solvent used to prepare the solution of PHEMA used to prepare the film of PHEMA studied. The edges of these regions are also darker due to the agglomeration of polymeric layers. The TEM micrograph of Na 4 shows the same darker domains, but also there is the presence of tubular structures, which are attributed to the CNTs used for the nanocomposite preparation. The length of these tubular structures is in order of microns. This length is typical of the CNTs. The described morphology of the Na 4 indicates that the CNTs$_{amine}$ are dispersed in the polymeric matrix of PHEMA.

Preprints (www.preprints.org) | NOT PEER-REVIEWED | Posted: 3 August 2023 doi:10.20944/preprints202308.0317.v1

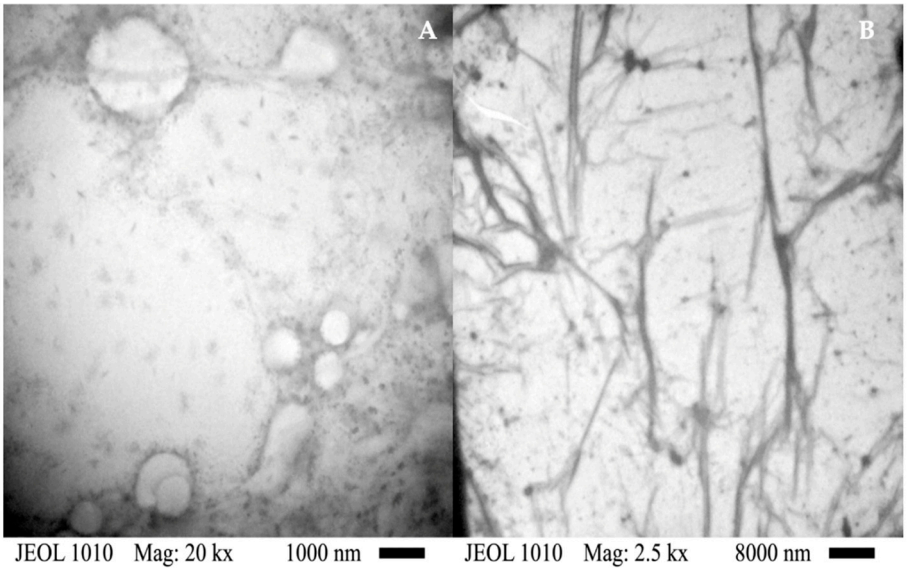

Figure 5. TEM micrographs of pure PHEMA (A) and Na 4 (B).

3.3. Thermal analysis of CNTs$_{amine}$/PHEMA nanocomposites

Figure 6 shows the DSC thermograms of pure PHEMA (Fig. 6A) and their nanocomposites (Figs. 6B, 6C, 6D, and 6E). PHEMA is an amorphous polymer. Their DSC thermogram shows only one thermal event: the glass transition relaxation. The measured glass transition temperature (T_g) of PHEMA is 75 ºC (348.15 K). For their nanocomposites, it is evident that the intensity of the change in the base-line of each thermogram caused by the glass transition relaxation decrease. Table 2 lists the glass transition temperature of all materials studied. The glass transition temperatures of the nanocomposites are larger than that of pure PHEMA. As expected, as the content of CNTs$_{amine}$ used in the nanocomposite preparation was higher, the T_g of the prepared nanocomposites was larger. The measured T_g of the Na 4 is 371.15 K (the highest of all nanocomposites studied), this temperature is 23 K major that the T_g of the pure PHEMA. The thermal behavior described is explained by the reduction in the mobility of the polymeric chains of PHEMA caused by the chemical bonds formed with the CNTs$_{amine}$. In this sense, this nanofiller acts as an agent that produces a constraint effect affecting the dynamics of the polymer chains of PHEMA. In a previous work of our research group, similar results were found for nanocomposites prepared with polyethylene glycol and CNTs functionalized with amine ending groups [20].

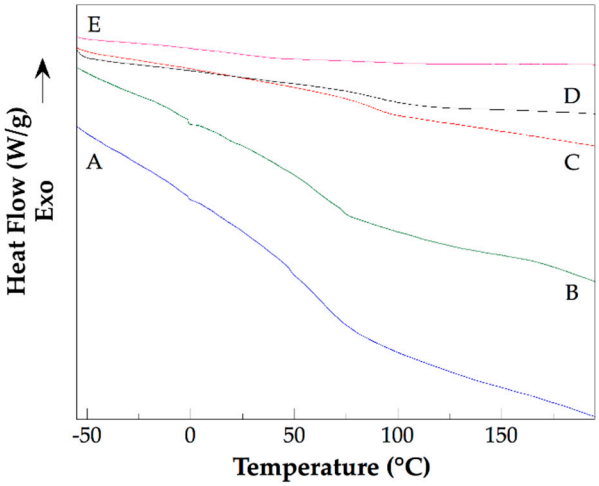

Figure 6. DSC thermograms of pure PHEMA (A), Na 2 (B), Na 1 (C), Na 4 (D), and Na 3 (E).

Preprints (www.preprints.org) | NOT PEER-REVIEWED | Posted: 3 August 2023 doi:10.20944/preprints202308.0317.v1

Table 2. Glass transition temperature of pure PHEMA, glass transition temperatures of $CNTs_{amine}$/PHEMA nanocomposites, and their grafting degree.

Sample	Tg (K)	Grafting degree
PHEMA	348.15	-
Na 1	361.15	42.0
Na 2	363.15	36.7
Na 3	370.15	30.3
Na 4	371.15	48.3

Figure 7 shows TGA thermograms of pure PHEMA and of the Na 2. The TGA thermogram of the other studied nanocomposites is very similar to that of Na 2. For pure PHEMA a small thermal decomposition was detected at temperatures below 265 ºC (538.15 K) and can be attributed mainly as due to the water loss. The main weight loss was observed in the range from ca. 265 ºC (538.15 K) to 500 ºC (773.15 K) and is due to the decomposition of the polymer chains of PHEMA. For Na 2 the thermal decomposition was developed in three stages: (i) the first from ca. 90 ºC (363.15 K) to 265 ºC (538.15 K) followed by a temperature range (from 265 ºC (538.15 K) to 275 ºC (548.15 K) in which a small loss of weight was recorded. (ii) The second stage was detected from 275 ºC (548.15 K) to 490 ºC (763.15 K), and (iii) the third from 490 ºC (763.15 K) to 800 ºC (1073.15 K). The weight loss of the first stage was 58.7%, while for the second stage was 31.2%. The first stage weight loss was attributed to degradation of the chemical groups attached to the surface of $CNTs_{amine}$ not linked to PHEMA chains, and the second stage loss was attributed to degradation of PHEMA chains chemically linked to the $CNTs_{amine}$. In a previous study, a similar thermal decomposition behavior was described for nanocomposites of PHEMA chains grafted to sidewalls of multiwalled carbon nanotubes (MWCNTs) prepared by fragmentation chain transfer (RAFT) polymerization, and reported elsewhere [32]. From the weight loss of the first and the second stages was calculated the degree of PHEMA chains grafted the CNTs in the Na 2. This degree resulted in 36.7%. Table 2 lists the grafting degree of nanocomposites studied. The Na 4 presented the higher grafting degree of all analyzed nanocomposites. This result is in accordance with the large amount of $CNTs_{amine}$ (1 wt. %) used in their preparation. Because as the amount of $CNTs_{amine}$ used to prepare the nanocomposites was larger, there are more chemical groups available to develop the grafting reaction with the PHEMA chains. Preparation of nanocomposites with polymer chains grafted to functionalized CNTs improves the dispersion of this nanofiller, which is a critical issue to obtain antimicrobial nanocomposites with desirable performance.

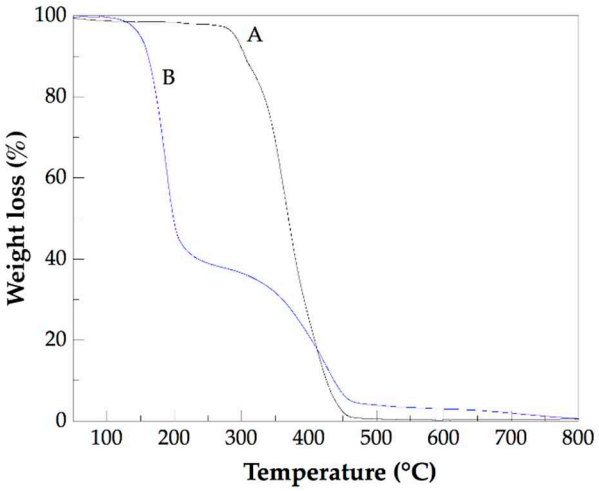

Figure 7. TGA thermograms of pure PHEMA (A) and Na 2 (B).

 doi:10.20944/preprints202308.0317.v1

3.4. Evaluation of the antifungal and antibacterial abilities of the CNTs$_{amine}$/PHEMA nanocomposites

Figure 8 shows four photographs of sections of Petri dishes where samples of Na 4 were inoculated with the fungus *Candida albicans* (A), or the bacteria *Pseudomona aeruginosa* (B), *Escherichia coli* (C), and *Staphylococcus aureus* (D). A difference to observed for the antibacterial tests of pure PHEMA, in mentioned photographs can observe an inhibition halo surrounding each sample of Na 4. This halo takes a colored appearance and marks the region where diffusion of chains PHEMA grafted to CNTs$_{amine}$ inhibit the growth of the fungus or the bacteria studied. The diameter size of the observed halo was 7 mm for tests with *C. albicans*, 4 mm for *P. aeruginosa*, 6 mm for *E. coli*, and 4 mm for *S. aureus*. Of the all nanocomposites studied, the diameter size of produced halo for the action of Na 4 was larger. These results indicated that the studied nanocomposites have antifungal and antibacterial abilities. However, these abilities are reduced and lower compared with respect to those of nanocomposites prepared also with CNTs and a biopolymer with antimicrobial properties. For example, chitosan is a biodegradable and biocompatible biopolymer with antimicrobial properties [33]. Nanocomposites of CNTs-chitosan shows synergistic effect in antimicrobial properties [34]. In this sense, CNTs functionalized with hydroxyl and carboxyl chemical groups had been used to prepare chitosan-based nanocomposites. These nanocomposites were prepared dispersing different amounts of functionalized CNTs in a solution of chitosan prepared with 40 mg of chitosan dissolved in 40 mL of 0.1 M aqueous acetic acid. The nanocomposite prepared with 50 mg of functionalized CNTs produced an inhibition halo of 18.20 ± 0.05 mm for *S. aureus*, 14.50 ± 0.08 mm for *E. coli*, and 19.20 ± 0.10 mm for *P. aeruginosa* [35]. A simple comparison of these results with the results of our study highlights the relevance of the polymer chosen as matrix of antimicrobial nanocomposites containing functionalized CNTs.

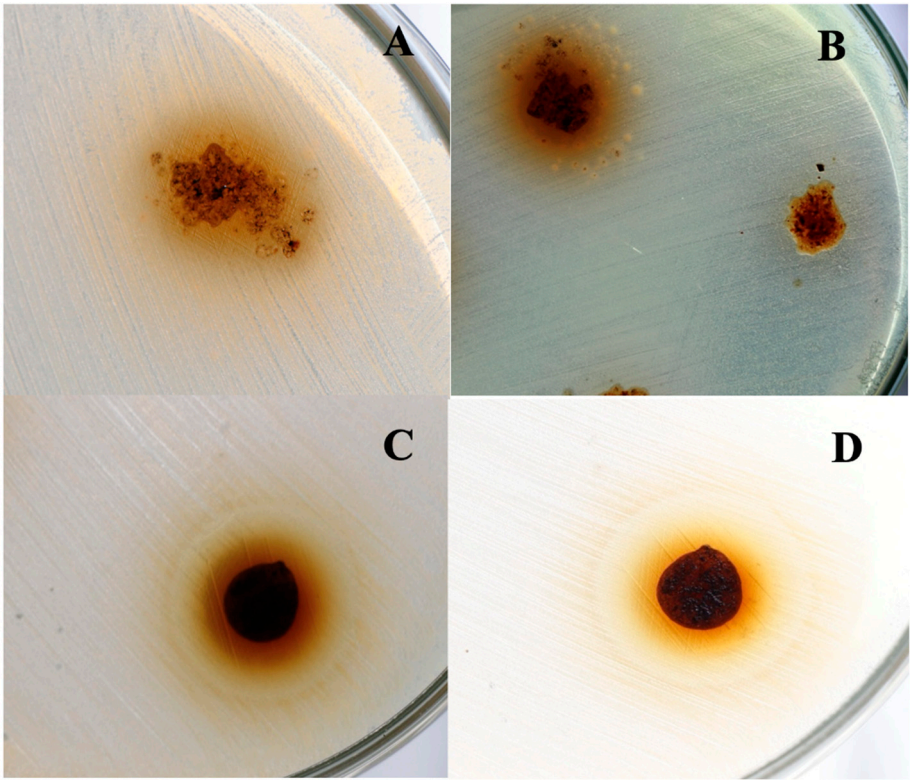

Figure 8. Photographs of Petri dishes in which is showed the inhibitory ability of Na 4 against *Candida albicans* ATCC 10231 (A), *Pseudomona aeruginosa* ATCC 9027 (B), *Escherichia coli* ATCC 25922 (C), and *Staphylococcus aureus* ATCC 6538 (D).

4. Conclusions

The preparation of CNTs$_{amine}$/PHEMA nanocomposites was carried out successfully. CNTs$_{amine}$ was obtained by functionalization of purified CNTs. An analysis by FT-IR and XPS spectroscopies

revealed that $CNTs_{amine}$ were linked through amide and ester groups to PHEMA chains. Micrographs of the prepared nanocomposites ofbtained by FE-SEM and TEM indicate that $CNTs_{amine}$ were immersed in the PHEMA polymer matrix without apparent segregation. An increment of the T_gs of prepared nanocomposites with respect to the T_g of pure PHEMA was detected by DSC. This increment was produced owing to a constraint effect induced by the $CNTs_{amine}$ attached to PHEMA chains. The grafting degree of PHEMA chains on the $CNTs_{amine}$ was determined by TGA. This degree enhances as the content of $CNTs_{amine}$ in the prepared nanocomposites increases. The $CNTs_{amine}$/PHEMA nanocomposites shows moderate antifungal ant antibacterial abilities against the fungus *C. albicans*, and the bacteria *P. aeruginosa*, *E. coli*, and *S. aureus*.

Author Contributions: Conceptualization, S.M.N.-D.; methodology, K.S.-G., A.G.A.-M., E.O.-G., and M.A.O.-R.; validation, L.A.C.-Z., A.G.A.-M., and S.M.N.-D.; formal analysis, K.S.-G., and S.M.N.-D.; investigation, K.S.-G.; resources, S.M.N.-D.; data curation, K.S.-G., and L.A.C.-Z.; writing—original draft preparation, S.M.N.-D.; writing—review and editing, K.S.-G., A.G.A.-M., E.O.-G., L.A.C.-Z., and S.M.N.-D.; visualization, K.S.-G., L.A.C.-Z., and S.M.N.-D.; supervision, S.M.N.-D.; project administration, S.M.N.-D.; funding acquisition, S.M.N.-D. All authors have read and agreed to the published version of the manuscript.

Funding: This research was funded by Consejo Nacional de Ciencia y Tecnología (CONACyT), grant number 101369.

Institutional Review Board Statement: Not applicable.

Data Availability Statement: The data presented in this study are available on request from the corresponding author.

Acknowledgments: The authors kindly acknowledge the Polymer Synthesis and Characterization Laboratory of the University of Guadalajara for their support in carrying out this work.

Conflicts of Interest: The authors declare no conflict of interest.

References

1. Zare, M.; Bigham, A.; Zare, M.; Luo, H., Ghomi, E.R.; Ramakrishna, S. pHEMA: An overview for biomedical applications. *Int. J. Mol. Sci.* **2021**, *22*, 6376.
2. Musgrave, C.S.A.; Fang, F. Contact lens materials: A materials science perspective. *Materials* **2019**, *12*, 261.
3. Ghanbarinia Firozjah, R.; Sadeghi, A.; Khoee, S. Ultrasonic De-cross-linking of the pH-and magneto-responsive PHEMA/PMMA microgel to janus nanoparticles: a new synthesis based on "grafting from"/"grafting to" polymerization. *ACS Omega* **2020**, *5*, 27119-27132.
4. Chen, L.; Tang, Y.; Zhao, K.; Liu, J.; Jiao, M.; Bai, H.; Wu, Z. HEMA-modified expandable p(MMA-AA) bone cement with dual water absorption networks. *Macromol. Mater. Eng.* **2020**, *305*, 1900752.
5. Wang, Y.; Chu, X.; Sun, Y.; Teng, P.; Xia, T.; Chen, Y. A convenient approach by using poly-(HEMA-co-NIPAM)/Cu^{2+} solution sol-gel transition for wound protection and healing. *J. Biomed. Mater. Res.* **2021**, *109*, 50-59.
6. Boni, R.; Ali, A.; Shavandi, A.; Clarkson, A.N. Current and novel polymeric biomaterials for neural tissue engineering. *J. Biomed. Sci.* **2018**, *25*, 90.
7. Jacob, S.; Nair, A.B.; Shah, J.; Sreeharsha, N.; Gupta, S.; Shinu, P. Emerging role of hydrogels in drug delivery systems, tissue engineering and wound management. *Pharmaceutics* **2021**, *13*, 357.
8. Das, D.; Pal, S. Dextrin/poly (HEMA): pH responsive porous hydrogel for controlled release of ciprofloxacin. *Int. J. Biol. Macromol.* **2015**, *72*, 171-178.
9. Chornopyshchuk, R.; Nagaichuk, V.; Gerashchenko, I.; Nazarchuk, H.; Kukolevska, O.; Chornopyshchuk, N.; Sidorenko, S. Antimicrobial properties of a new polymeric based on poly(2-hydroxyethyl methacrylate). *Acta Biomed.* **2022**, *93*, e2022012.
10. Ergene, C.; Yasuhara, K.; Palermo, E.F. Biomimetic antimicrobial polymers: recent advances in molecular design. *Polym. Chem.* **2018**, *9*, 2407-2427.
11. Kumar, N.A.; Ganapathy, H.S.; Kim, J.S.; Jeong, Y.S.; Jeong, Y.T. Preparation of poly 2-hydroxyethyl methacrylate functionalized carbon nanotubes as novel biomaterial nanocomposites. *Eur. Polym. J.* **2008**, *44*, 579-586.
12. Prashantha, K.; Rashmi, B.J.; Lee, J.H. Preparation and characterization of carbon nanotube filled poly(2-hydroxyethylmethacrylate) nanocomposites. *High Perform. Polym.* **2012**, *25*, 97-103.
13. Mocan, T.; Matea, C.T.; Pop, T.; Mosteanu, O.; Buzoianu, A.D.; Suciu, S.; Puia, C.; Zdrehus, C.; Iancu, C.; Mocan, L. Carbon nanotubes as anti-bacterial agents. *Cell. Mol. Life Sci.* **2017**, *74*, 3467-3479.
14. Wang, X; Li, Q.; Xie, J.; Jin, Z.; Wang, J.; Li, Y.; Jiang, K., Fan, S. Fabrication of ultralong and electrically uniform single-walled carbon nanotubes on clean substrates. *Nano Lett.* **2009**, *9*, 3137-3141.

15. Díez-Pascual, A.M. Antibacterial activity of nanomaterials. *Nanomaterials* **2018**, *8*, 359.
16. Saleemi, M.A.; Kong, Y.L.; Yong, P.V.C.; Wong, E.H. An overview of antimicrobial properties of carbon nanotubes-based nanocomposites. *Ad. Pharm. Bull.* **2022**, *12*, 449-465.
17. Díez-Pascual, A. M. State of the art in the antibacterial and antiviral applications of carbon-based polymeric nanocomposites. *Int. J. Mol Sci.* **2021**, 22, 10511.
18. Gómez-Vázquez, D.; Cajero-Zul, L.R.; Torres-Ávalos J.A.; Sandoval-García, K.; Cortés-Ortega, J.A.; López-Dellamary, F.A.; Soltero-Martínez, J.F.A.; Martínea-Richa, A.; Nuño-Donlucas, S.M. Homogeneous hydrogels made with acrylic acid, acrylamide and chemically functionalized carbon nanotubes. *J. Macromol. Sci., Part A* **2019**, *56*, 417-428.
19. Rúan-Esparza, L.; Soto, V.; Gómez-Salazar, S.; Rabelero, M.; Ávalos-Borja, M. Luna-Bárcenas, G.; Prokhorov, E.; Nuño-Donlucas, S.M. Poly[ethylene-co-(acrylic acid)]-based nanocomposites: Thermal and mechanical properties and their structural characteristics studied by Raman spectroscopy. *Polym. Compos.* **2011**, *32*, 1182-1189.
20. Sandoval-García, K.; Alvarado-Mendoza, A.G.; Jiménez-Avalos, J.A.; García-Carvajal, Z.Y.; Olea-Rodríguez, M.A.; Cajero-Zul, L.R.; Nuño-Donlucas, S.M. Synthesis, characterization and evaluation of the toxicity, drug release ability and antibacterial capacity of nanocomposites of polyethylene glycol and functionalized carbon nanotubes. *J. Macromol. Sci., Part A* **2022**, *59*, 889-903.
21. Silva-Jara, J.M.; Manríquez-González, R.; López-Dellamary, F.A.; Puig, J.E.; Nuño-Donlucas, S.M. Semi-continuos heterophase polymerization to synthesize nanocomposites of poly(acrylic acid)-functionalized carbon nanotubes. *J. Macromol. Sci., Part A* **2015**, *52*, 732-744.
22. Xia, R.; Li, M.; Zhang, Y.; Qian, J.; Yuan, X. Surface modification of MWCNTs with BA-MMA-GMA terpolymer by single-step grafting technique. *J. Appl. Polym. Sci.* **2011**, *119*, 282-289.
23. Herrera-Gomez, A.; Bravo-Sanchez, M.; Ceballos-Sanchez, O.; Vazquez-Lepe, M.O. Practical Methods for Background Subtraction in Photoemission Spectra. *Surf. Interface Anal.* **2014**, *46*, 897-905.
24. Clinical and Laboratory Standards Institute (CLSI). Performance Standards for Antimicrobial Susceptibility Testing. In Twenty-Fourth Informational Supplement. CLSI: Wayne, PA, 2014.
25. Vargün, E.; Usanmaz, A. Degradation of poly(2-hydroxyethyl methacrylate) obtained by radiation in aqueous solution. *J. Macromol. Sci., Part A* **2010**, *47*, 882-891.
26. Beamson, G.; Briggs, D. *High Resolution XPS of Organic Polymers: The Scienta ESCA300 Database*, 1st ed.; Wiley: Chishester, UK, 1992; pp. 110-117.
27. Tuccitto, N.; Spitaleri, L.; Li Destri, G.; Pappalardo, A.; Gulino, A.; Trusso Sfrazzetto, G. Supramolecular sensing of a chemical warfare agents by functionalized carbon nanoparticles. *Molecules* **2020**, *25*, 5731.
28. Andrade-Melecio, H.A.; Antolín-Cerón, V.H.; Alvarado-Mendoza, A.G.; Vázquez-Lepe, M.; Barrera-Rivera, K.A.; Martínez-Richa, A.; Nuño-Donlucas, S.M. Semi-continuous heterophase polymerization to synthesize poly(methacrylic acid)-based nanocomposites for drug delivery. *Polymers* **2022**, *14*, 1195.
29. Islam, Md.R.; Bach, L.G.; Lim, K.T. Poly(2-hydroxyethyl methacrylate) grafted halloysite nanotubes as a molecular host matrix for luminescent ions prepared by surface-initiated RAFT polymerization and coordination chemistry. *Appl. Surf. Sci.* **2013**, *276*, 298-305.
30. Nguyen, V.H.; Haldorai, Y.; Pham, Q.L.; Shim, J.-J. Supercritical fluid mediated synthesis of poly(2-hydroxyethyl methacrylate)/Fe_3O_4 hybrid nanocomposite. *Mater. Sci. Eng. B* **2011**, *176*, 773-778.
31. Moura, D.; Pereira, A.T.; Ferreira, H.P.; Barrias, C.C.; Magalhães, F.D.; Bergmeister, H.; Gonçalves, I.C. Poly(2-hydroxyethyl methacrylate) hydrogels containing graphene-based materials for blood-contacting applications: From soft inert to strong degradable material. *Acta Biomater.* **2023**, *164*, 253-268.
32. Pei, X.; Hao, J.; Liu, W. Preparation and characterization of carbon nanotubes-polymer/Ag hybrid nanocomposites via surface RAFT polymerization. *J. Phys. Chem. C.* **2007**, *111*, 2947-2952.
33. Mokhena, T.C.; Jacobs, V.; Luyt, A.S. A review on electrospun bio-based polymers for water treatment. *EXPRESS Polym. Lett.* **2015**, *9*, 839-880.
34. Azizi-Lalabadi, M.; Hashemi, H.; Feng, J.; Jafari, S.M. Carbon nanomaterials against pathogenes; the antimicrobial activity of carbon nanotubes, graphene/graphene oxide, fullerenes, and their nanocomposites. *Adv. Colloid Interface Sci.* **2020**, *284*, 102250.
35. El-Tohamy, N.; Attia, M.; Easa, S.M.; Awad, N.M. Characterization and evaluation of nanocomposites chitosan-multiwalled carbon nanotubes as broad-spectrum antibacterial agent. *J. Sci. Res. Sci.* **2018**, *35*, 16-27.